Journal of Applied and Natural Science
14(4), 1327 - 1336 (2022)
ISSN : 0974-9411 (Print), 2231-5209 (Online)
journals.ansfoundation.org

Research Article

Performance evaluation of Satellite-based actual evapotranspiration technique

R. S. Makar*
Soils and Water Use Department, Agricultural and Biological Research Institute, National Research Centre, Dokki, Cairo, Egypt
M. Faisal
Drainage Research Institute, National Water Research Center, Egypt

*Corresponding author. Email: randa_sgmm@yahoo.com

Article Info
https://doi.org/10.31018/jans.v14i4.3967
Received: August 23, 2022
Revised: November 14, 2022
Accepted: November 19, 2022

How to Cite
Maker, R.S. and Faisal, M. (2022). Performance evaluation of Satellite-based actual evapotranspiration technique. *Journal of Applied and Natural Science*, 14(4), 1327 - 1336. https://doi.org/10.31018/jans.v14i4.3967

Abstract
Estimating crop evapotranspiration is vital for the calculation of irrigation water requirements. Remote sensing data have proven to be a valuable and efficient tool for estimating evapotranspiration. It has been used intensively over the past decade due to free, high temporal and spectral resolution data availability. The main aim of this study was to estimate the evapotranspiration (ET) over a selected area in El-Beheira governorate, Egypt based on the Simplified Surface Energy Balance Index (S-SEBI) using nine Landsat-8 images acquired from January to December 2020. The performance of the studied method was compared with the CROPWAT-8 model. The results revealed the acceptable accuracy of the ET estimated from S-SEBI algorithms with Landsat 8 images according to the coefficient of determination (r^2 = 0.82) and root mean square error (RMSE = 0.53 mm/day). Therefore, it is recommended to use the S-SEBI to calculate the spatial evapotranspiration distribution using Landsat-8 images to provide the required information for determining irrigation water requirements and suggesting an efficient water management strategy.

Keywords: Crop evapotranspiration, CROPWAT-8 model, Remote sensing, Simplified surface energy balance index (S-SEBI)

INTRODUCTION

Agricultural water use in Egypt consumes about 85% of the total national available water. Therefore, efficient irrigation water use estimates are essential to ensure an efficient water resources management, especially under the current water scarcity (Ezz and Abdelwares, 2020). Especially with the increased population and under the fixed limited water resources of Egypt, which is mainly the Nile River and with the predicted climate changes, it is expected that the water resources will become scarcer. Moreover, efficient irrigation water use for different crops requires the estimation of evapotranspiration (Rawata *et al.*, 2019).

Higher resolution satellite images, with modern sensors that measure additional variables, provide an increasingly popular approach for spatio-temporal estimation of Actual evapotranspiration (ETa). This resulted in many attempts to develop algorithms to estimate Eta using remote sensing data. However, the scarcity of ground-based measured data makes validation of such algorithms a remarkable challenge. Validation of such algorithms will enable the decision-makers to use remote sensing information to enhance water use efficiency (Ayyad *et al.*, 2019).

Since the early 1970's, many studies have shown the importance of remote sensing data for providing spatio-temporal information on actual evapotranspiration (Li *et al.*, 2009). Furthermore, recent satellite images with higher temporal and spectral resolutions have been introduced in the past few decades. Much of this data became more available at no cost, making it possible to estimate actual evapotranspiration (ETa) (Kumar *et al.*, 2020). Improvements in the methodologies for estimating ETa from satellite data were developed over recent decades, which reduced the need for intensive ground-based measurements (Senay *et al.*, 2013).

Many studies were conducted to develop methods that used remote sensing data to estimate crop evapotranspiration (ET). Complicated models such as SEBAL (Surface Energy Balance Algorithm for Land) and its deviations, such as METRIC (Mapping Evapotranspiration at High Resolution with Internalized Calibration), have been used intensively. Reyes-González *et al.*

(2019) utilized data from Landsat 7 and Landsat 8 with the METRIC model and reached r2 = 0.89 and RMSE = 0.71 mm/day compared with in-situ measurements. Similar results were obtained by Mondal *et al.* (2022) with Landsat-8 data and they also recommended exploring the application of the methodology with finer temporal resolution satellites such as MODIS (Moderate Resolution Imaging Spectro-radiometer) to reproduce accurate estimates of ET. Bezerra *et al.* (2015) evaluated the accuracy of estimation of daily actual evapotranspiration (ETa) obtained by TM Landsat-5 images acquired with both the SEBAL (Surface Energy Balance Algorithm for Land) and SSEB (Simplified Surface Energy Balance) algorithms. Their results showed acceptable accuracy between ET estimates obtained from remote sensing and in-situ data. In addition, they showed that SSEB algorithm is an important tool for ET analysis in semi-arid regions because it only needs an average temperature of the "hot" and "cold" pixels. Moreover, they reported that SSEB is a simpler algorithm, unlike SEBAL algorithm that is more complex and needs an iterative process for solving the sensible heat flux values. Abdel Kader *et al.* (2015) estimated ET values using the Surface Energy Balance System (SEBS model) for various crops using Landsat ETM+7 images on the farm scale. They stated that the main advantage of using the SEBS is the possibility of producing water balance maps for the study area for the farm scale and even for smaller areas and tracking water use in the study area over time. Furthermore, Kumar *et al.*(2020) used Landsat-8 and the Simplified Surface Energy Balance Index (S-SEBI) to estimate ET. The results showed that the S-SEBI performed well compared to in-situ data (r2 = 0.90). Their results revealed the applicability and accuracy of using the S-SEBI method with remote sensing-based ET data for water resources management in a command area with scarcedata. Hence, the present research aimed to evaluate the use of this method in estimating ET over a selected area in Egypt utilizing Landsat-8 data.

MATERIALS AND METHODS

Study area

An area was selected for method application that covers about 116700 feddans (1 feddan = 4200 m^2) and is located about 84 km to the north-west of Cairo, in El-Beheira governorate, Egypt. This area is considered a newly reclaimed area (about 20 years) and cultivated mostly vegetables and orchards, in addition to wheat and Egyptian clover in winter. Nevertheless, a smaller area was selected for method validation within the application area and covers about 228.5 feddans (Fig. 1). This area was irrigated from groundwater via a drip irrigation system. The area is mostly covered by citrus and olive, in addition to a small area of field crops; the rest are bare soils. The meteorological normal were acquired for 2020 of the study area from the National Aeronautics and Space and Administration Prediction of Worldwide Energy Resource (NASA POWER) (Table 1). The data were available for a resolution of 0.5◦ latitude by 0.5◦ longitude globally (Rodrigues and Braga, 2021) at NASA POWER's website (https://power.larc.nasa.gov/).

The data revealed that the mean annual maximum temperature was 33.8°C and mean annual minimum tem-

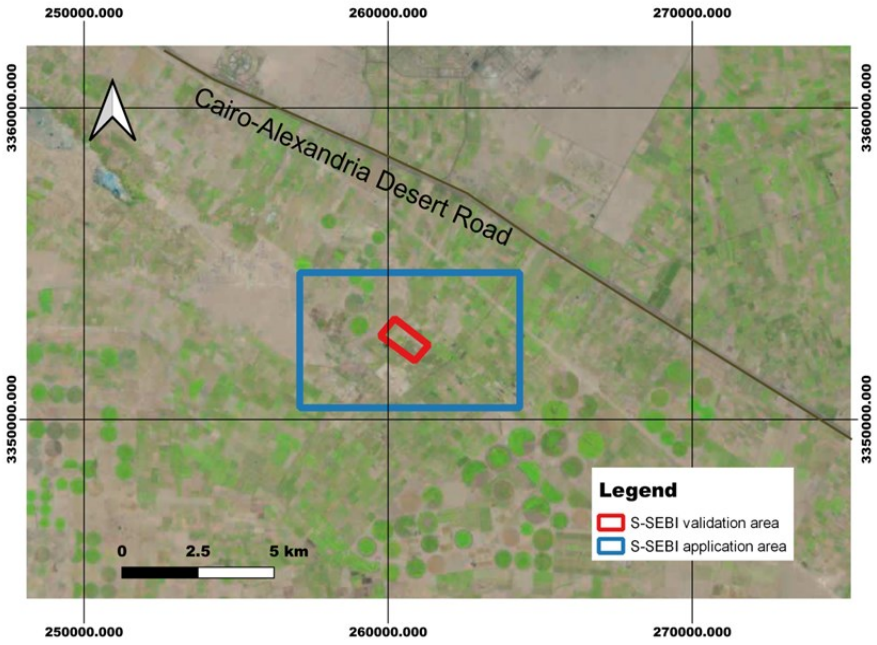

Fig. 1. *Location of the studied area within El-Beheira governorate, Egypt*

Table 1. Meteorological data of the studied area (1991-2020)

Month	Temperature °C		Humidity (%)	Wind (km/ day)	Precipitation (mm)	Sunshine hours
	Tmax	Tmin				
Jan.	23.4	12.0	65	240	6.1	10.4
Feb.	26.8	12.1	61	243	5.4	10.4
Mar.	31.9	14.8	56	256	6.9	10.5
Apr.	37.1	18.3	49	269	7.6	10.5
May	33.5	16.0	54	259	0.5	10.5
Jun.	41.1	22.4	47	286	0.5	10.5
Jul.	40.9	23.7	50	279	0.2	10.5
Aug.	39.8	23.9	52	259	0.0	10.6
Sep.	38.8	23.1	54	252	0.2	10.6
Oct.	36.1	21.4	58	237	2.4	10.6
Nov.	30.7	17.9	61	229	6.3	10.6
Dec.	25.4	14.5	65	236	3.3	10.7
Average/	33.8	18.3	56	254	39.4	10.5

perature was 18.3°C. The hottest month was June (41.1°C) and the coldest was January (12.0°C). The mean annual relative humidity is 56 %. The area receives a total amount of rainfall of approximately 39.4 mm/year. The rainy months extend mainly from October to April. The annual monthly total rainfall varies between 0.0 mm in August and 6.3 mm in December. The annual mean wind speed is 254 km/day and the highest value was recorded in June (286 km/day), while the lowest was in November (229 km/day). The sunshine hours ranged from 10.4 to 10.7, with an average of 10.5 hours.

Remotely sensed data

According to the United States Geological Survey (United States Geological Survey, 2019), Landsat-8 is stationed at a Sun-synchronous orbit at 705 km, with a revisit cycle of 16 day. This satellite has two sensors: the Operational Land Imager (OLI) and the Thermal Infrared Sensor (TIRS) and consists of nine bands. There were OLI deliver images of 30 meters spatial resolution (visible, NIR, SWIR); and one high-resolution panchromatic band at 15 meters' resolution, while the TIRS delivered two thermal bands at 100 m resolution. The area is located on Landsat-8 Path 177 and row 39. A scene was selected for each month in 2020 except for January, March and November; nocloud clear images were available for the study area (Table 2). Accordingly, nine Landsat 8 images were selected to evaluate the potentiality and efficiency of the S-SEBI in estimating ET for selected crops in the study area. Landsat-8 data used in the present study were acquired as Level 1 data products in GeoTIFF data format from the United States Geological Survey (USGS) website (https://earthexplorer.usgs.gov/).

Moreover, the Digital Elevation Model (DEM) produced from Shuttle Radar Topography Mission (SRTM) with one Arc-Second resolution (approximately 30 meters) was downloaded from the United States Geological Survey (USGS) website (https://earthexplorer.usgs.gov) and used in this research. The data revealed that most of the north western part of the study area was almost flat and ranged between -6 and 10 m while the southeastern part ranged from 10-50 m (Fig. 2).

Simplified surface energy balance index (S-SEBI)

The S-SEBI is a remote sensing energy balance model to estimate surface energy fluxes from remote sensing measurements (Basit *et al*., 2018). The model was developed by Roerink *et al.* (2000) that estimates ET by using surface reflectance and the land surface temperature(LST) from dry and wet pixels (Bezerra *et al*., 2015, Basit *et al*., 2018, Kumar *et al*., 2020 and Kumar *et al*., 2021). In the S-SEBI approach, the actual ET (mm/day) can be estimated as follows (Kumar *et al*., 2020).

$$ET = \frac{86400 \times 10^3}{\lambda \times \rho_w} \Lambda R_n \quad \text{Eq. 1}$$

where λ = latent heat of vaporization (J/kg), Λ = evaporative fraction, and ρ_w= the density of water (kg/m^3) and R_n is the net radiation flux (Wm^{-2}).On the other hand, R_n was adopted from Sobrino *et al.* (2021) as follows

$$R_n = (1 - \alpha)\, R_g + \varepsilon\, R_a - \varepsilon\, \sigma\, T_s^4 \quad \text{Eq. 2}$$

R_g and R_a is the incident solar radiation and the longwave radiation in Wm^{-2}, respectively, α is the surface albedo; ε is the surface emissivity; T_s is the land surface temperature; and σ is the Stefan–Boltzmann constant. R_g, R_a and T_s have been obtained using the metrological data from the NASA POWER website.

Λ was calculated according to Roerink *et al.* (2000) which used two extreme surface reflectance to surface temperature relationships acquired from plotting two-dimensional scatter plot of surface reflectance (albedo) against the land surface temperature (LST) (Fig. 3). In this approach, two extreme pixels (wet and dry pixel) were used and Λ is calculated as:

$$\Lambda = \frac{(T_H - Ts)}{(T_H - T_c)} \quad \text{Eq. 3}$$

Table 2. Dates of the selected Landsat-8 data

Month	Day	Month	Day	Month	Day
February	3-2-2020	June	10-6-2020	September	30-9-2020
April	23-4-2020	July	28-7-2020	October	16-10-2020
May	25-5-2020	August	29-8-2020	December	3-12-2020

where T_H is the maximum LST on hot edge temperature, controlled by the radiation as a linear function of the surface albedo, T_s is the LST, and T_C is the minimum LST on cold edge, controlled by evaporation as a function of surface albedo.

Landsat-8 data processing

Data pre-processing

A radiometric correction was done by transforming the Digital Number (DN) values to radiance or reflectance values using the methodology suggested by USGS. The level-1 DN values are converted into top of atmosphere (TOA) reflectance using Equations 4 and 5 and only Landsat-8 bands 2-7 were used.

$$\rho_{re} = (M_{re} \times Q) + A_{re} \quad \text{Eq. 4}$$

$$\rho_{re'} = \frac{\rho_{re}}{sin\theta SE} \quad \text{Eq. 5}$$

Where, ρ_{re} is the TOA reflectance, M_{re} is the band multiplicative value, A_{re} is the band additive value, Q is the digital numbers (DN) of the Landsat satellite bands, ρre′ is the TOA planetary reflectance and θSE is the sun elevation angle.

The brightness temperature was calculated using the digital numbers (DNs) of the first thermal infrared bands, namely Landsat-8 band 10, as suggested by the USGS. Firstly, the DNs were converted to TOA spectral radiance as in equation 6. Then, the brightness temperature was computed using spectral radiance as in equation 7.

$$\rho_{ra} = (M_{ra} \times Q) + A_{ra} \quad \text{Eq. 6}$$

$$T = \frac{\mathrm{K2}}{\ln\left(1+\frac{K1}{\rho_{ra}}\right)} \quad \text{Eq. 7}$$

Where ρ_{ra}= TOA spectral radiance, M_{ra}=Band multiplicative factor, *T* = Top of atmosphere brightness temperature, A_{ra}=Band additive factor, *Q* = pixel digital numbers (DN),andK_1*and* K_2 are both Band-specific thermal conversion constants. M_{re}, A_{re}, θSE, M_{ra},A_{ra}, K_1, and K_2 were acquired from the documents enclosed with the downloaded Landsat-8 data.

Model variable preparation from remote sensing data

Surface albedo

Surface albedo can be defined as the property of the body causing it to reflect and emit a specific portion of the incident radiation in a broad spectral range (Kukla, 1981). It is also defined as the ratio of the reflected solar radiation to the incident solar short-wave radiation at the surface. The surface albedo was calculated by integrating band reflectance within the short-wave spectrum using a weighting function (Allen *et al.*, 2007).

$$\alpha = \frac{\alpha_{TOA} - \alpha_{Atm}}{\tau_{sw}\,2} \quad \text{Eq. 8}$$

Where αis the surface albedo, α_{Atm} is the portion of solar radiation reflected by the atmosphere and it was adopted to 0.03 according to Bastiaanssen (2000), α_{TOA} is the top of the atmosphere's albedo. On the other hand, τ_{sw} is the transmissivity of atmosphere and was calculated according to Sobrino *et al.* (2003) for any clear sky day.

$$\tau_{sw} = 0.75 + 2 \times 10^{-5}(h) \quad \text{Eq. 9}$$

where h is the surface height above sea level (m).

The top of the atmosphere's albedo (α_{TOA}) is calculated according to Alves *et al.* (2017) as follows:

$$\alpha_{TOA} = \Sigma(\omega n \times \rho_{re'}) \quad \text{Eq. 10}$$

Where $\rho_{re'}$ is the TOA planetary reflectance of band n and $\omega n$are the weigh coefficient of the different Landsat-8 bands (n) (Table 3) (https://www.usgs.gov/landsat-missions/using-usgs-landsat-level-1-data-product).

Surface emissivity

Land surface emissivity (*ε*) is a proportionality factor that scales blackbody radiance to predict emitted radiance, and it is the efficiency of transmitting thermal energy across the surface into the atmosphere (Sobrino *et al.*, 2008). Various methods were developed to produce surface emissivity among which is the $NDVI^{THM}$, which was introduced by Sobrino and Raissouni (2000). This method uses certain NDVI values (thresholds) to calculate the surface emissivity. The present study applied the $S\text{-}NDVI^{THM}$ (Simplified-$NDVI^{THM}$) which is a simplified version of the $NDVI^{THM}$ as proposed by Sobrino *et al.* (2008).

$$\varepsilon = \begin{cases} \varepsilon s, & NDVI < NDVIs \\ \varepsilon s + (\varepsilon v - \varepsilon s)P_v, & NDVIs \le NDVIs \le NDVIv \\ \varepsilon v\ , & NDVI > NDVIv \end{cases} \quad \text{Eq.11}$$

where εs and εv are soil and vegetation emissivities of the thermal bands, respectively, *Pv* is the proportion of vegetation. The land surface emissivity of band 10 is 0.964 and 0.984 for the soil and vegetation, respectively (Sobrino *et al.*, 2001).

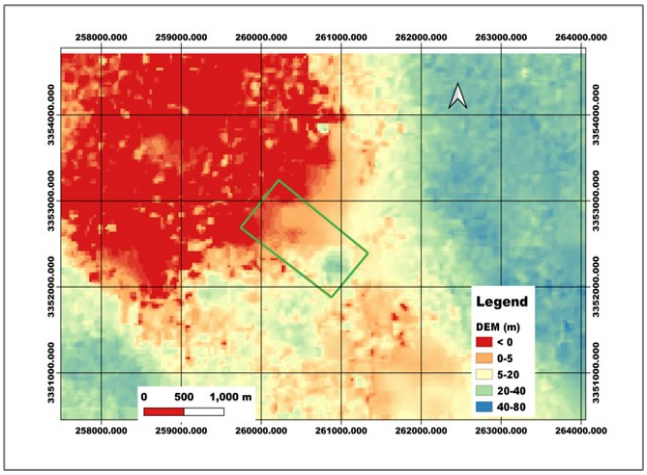

Fig. 2. *DEM of the study area*

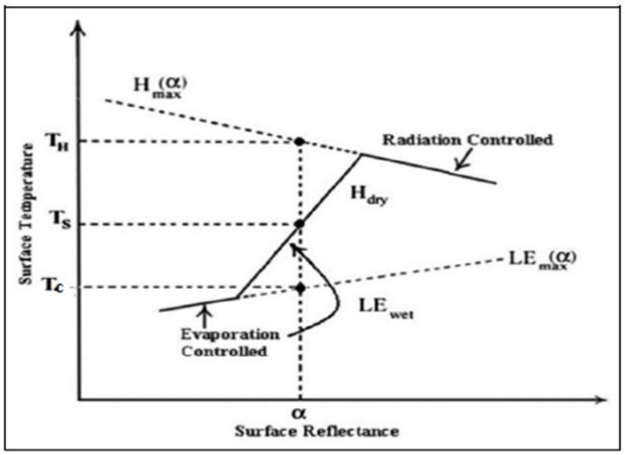

Fig. 3. *Scatter plot of the surface temperature and surface reflectance (modified after Roerink et al., 2000)*

NDVI is the most often used vegetation index and has been used in monitoring global vegetation coverage over the past two decades (Jiang *et al.*, 2006). NDVI was calculated according to Rouse *et al.* (1974).

$$NDVI = \frac{\rho NIR - \rho RED}{\rho NIR + \rho RED} \quad \text{Eq.12}$$

Where ρNIR is the near-infrared reflectance and ρ*RED* refers to the red reflectance NDVIs and NDVIv are, the NDVI for soil and vegetation, respectively. These values were suggested by (Sobrino and Raissouni, 2000) as NDVIs = 0.2 and NDVIv = 0.5. Pv is the proportion of vegetation ranging between 0 and 1 and was calculated using the NDVI according to Carlson and Ripley (1997).

$$P_v = P\left(\frac{NDVI - NDVI_S}{NDVI_v - NDVI_S}\right)^2 \quad \text{Eq. 13}$$

Performance evaluation of S-SEBI

To evaluate the effectiveness of the S-SEBI method, the CROPWAT-8 model was used. CROPWAT model is an empirical process-based crop model used to calculate crop water and irrigation requirements and permits the development of irrigation schedules under different management conditions (Food and Agriculture Organization, 2009). The model uses Penman–Monteith method as a base for calculating evapotranspiration and irrigation water requirements for separate crops and croprotations (Vozhehova*et al.*, 2018). For the calculation of the ET the model requires the metrological data of the studied area as well as specific crop data. The Meteorological data were acquired from NASA POWER, as mentioned before.On the other hand, the crop data such as Kc, growth stages, root depth etc. were collected according to Allen *et al.* (1998).

Two performance indicators were used in this research namely; the coefficient of determination (r2), and root-mean-squared error (RMSE). Therefore, the mean ET values were calculated from S-SEBI for both citrus and olive in the study area (as they covered most of the validation area) and compared with the values produced from the CROPWAT-8 model.

RESULTS AND DISCUSSION

Development of the land cover map for the model validation area

Specific crops must be identified in the study area to evaluate the ET produced from the S-SEBI using the CROPWAT model. Therefore, a smaller area was selected and the land cover class (LC) was identified according to the method suggested by Makar *et al.* (2022). The method recommended using two types of principle component analysis (PCA) on a series of remote sensing images and using only the first and second resulting PCA for classification to ensure high classification accuracy.Four Landsat-8 images were selected for land cover (LC) map development which were acquired on 03/02/2020, 23/04/2020, 28/07/2020 and 16/10/2020.

To validate the suggested method, the correlation matrix was first developed to investigate the correlation between the different Landsat-8 bands (from 2-7). All the images showed the same trend and examples of the results of the two images are shown in Tables 4

Table 3. Weigh coefficient (ωn) to the planetary albedo for LANDSAT-8 images

Bands	Band 2	Band 3	Band 4	Band 5	Band 6	Band 7
ωn	0.301	0.276	0.234	0.142	0.036	0.012

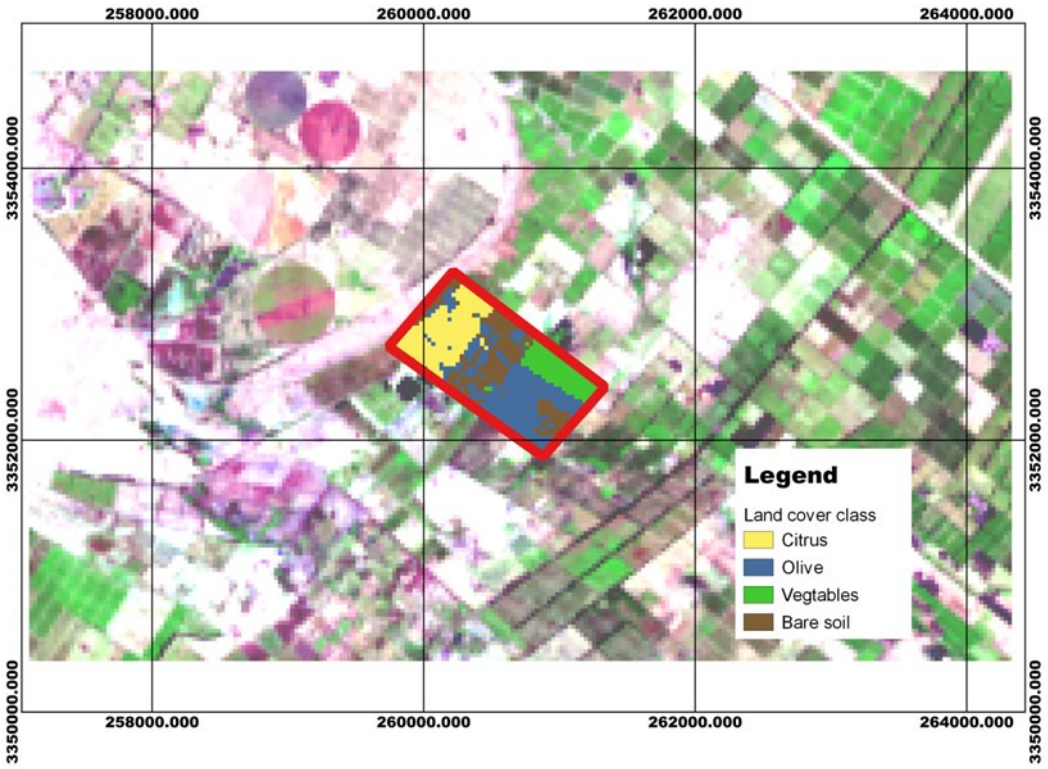

Fig. 4. *Land cover of S-SEBI validation area*

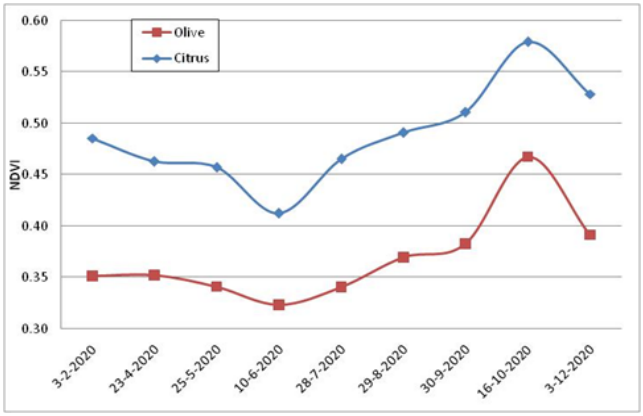

Fig. 5. *Sequential average NDVI values of the studied crops*

and 5 for dates 23/04/2020 and 16/10/2020, respectively. Within this matrix, the correlation coefficient between the reflectance of each pair of satellite bands is computed for each pixel in the images. In the studied images, all band pairs had strong correlation with each other except band five (the near-infrared band), which showed moderate to strong correlation with the other bands. Based on field work, four LC classes were distinguished. These classes included citrus, olive, bare soils and vegetables. Within the study area, 10 training sets (locations) were selected for the land use/ cover classification. Accordingly, a PCA was performed on the four used images (Table 6).The results revealed that the first PCA represented most of the data variability (89.33 – 95.25%). Then, a second PCA was performed on the six images from stacking the matching bands of the four selected dates to enhance the classification accuracy further and utilize the effect of the different characteristics of the vegetation cover throughout the growing season (Table 7). The first PCA account was for about 87.23-97.05 % of the data variability. Therefore, instead of using the first two PCAs as

Table 4. Correlation matrix between the Landsat 8 bands acquired on 23rd of April

Band	B2	B3	B4	B5	B6	B7
B2	1.000					
B3	0.983	1.000				
B4	0.959	0.984	1.000			
B5	0.577	0.622	0.545	1.000		
B6	0.903	0.933	0.951	0.542	1.000	
B7	0.905	0.937	0.955	0.482	0.984	1.000

Table 5. Correlation matrix between the Landsat 8 bands acquired on 16th of October

Band	B2	B3	B4	B5	B6	B7
B2	1.000					
B3	0.990	1.000				
B4	0.972	0.991	1.000			
B5	0.813	0.847	0.834	1.000		
B6	0.918	0.943	0.961	0.845	1.000	
B7	0.933	0.956	0.970	0.805	0.984	1.000

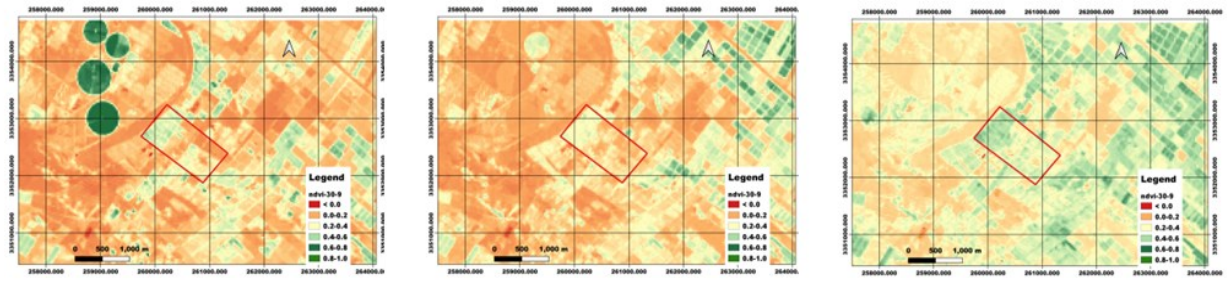

Fig. 6. *NDVI maps of the studied area (A. 3rd February, B. 10th June and C. 16th October)*

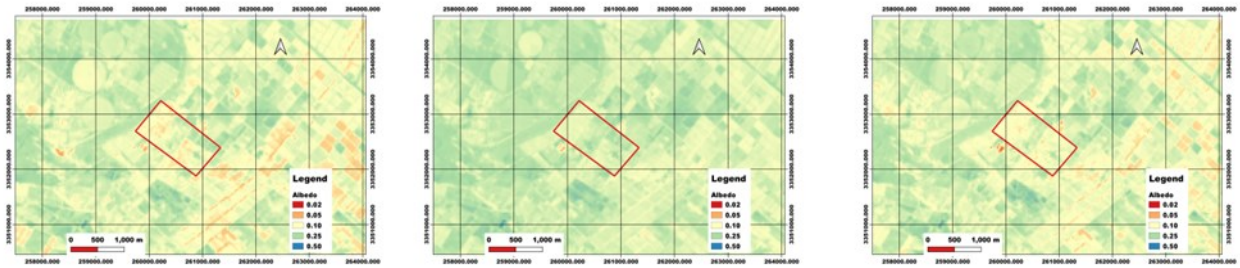

Fig. 7.*Example surface albedo maps of the studied area (A. 3rd February, B. 10th June and C. 16th October)*

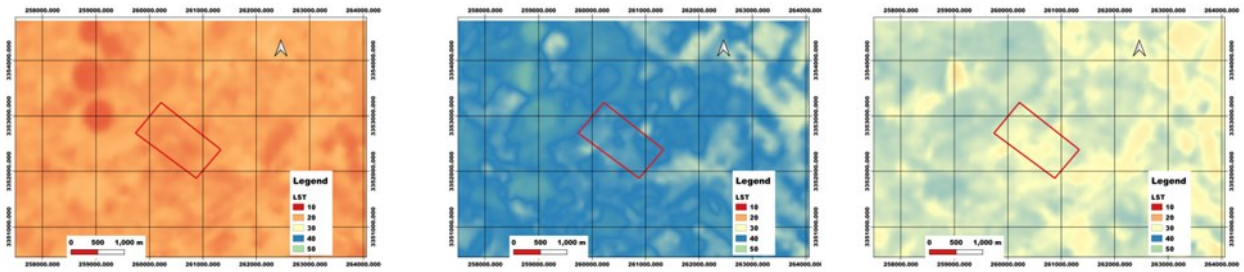

Fig. 8. *Example LST maps of the studied area (A. 3rd February, B. 10th June and C. 16th October)*

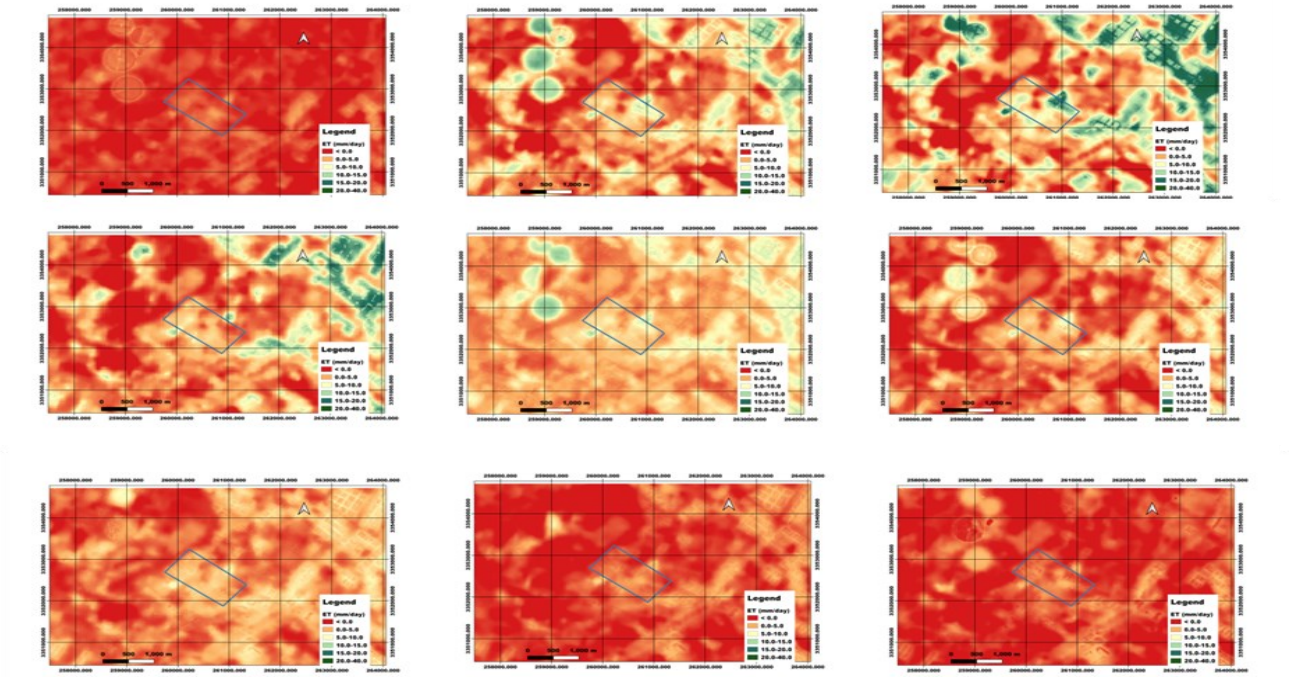

Fig. 9. *ET map of the studied area (A. 3rd Feb., B. 23rd Apr., C. 25th May, D. 10th Jun., E. 28th Jul., F. 28th Aug., G. 30th Sep., H. 16th Oct., 3rd Dec.)*

Table 6. Eigenvectors of the covariance matrix of the four Landsat images

Date	PCA1	PCA2	PCA 3-6
3/2/2020	89.33	8.35	2.32
23/04/2020	94.27	3.25	2.48
28/7/2020	92.36	5.06	2.57
16/10/2020	95.25	2.76	1.99

Table 7. Eigenvectors of the covariance matrix of the nine bands images

Band\PCA	PCA1	PCA2	PCA 3-4
B2	97.05	2.26	0.68
B3	94.61	4.33	1.06
B4	91.55	6.57	1.89
B5	97.04	2.34	0.62
B6	92.06	5.95	1.98
B7	87.23	9.84	2.93

recommended by Makar *et al.* (2022), only the first PCA resulting from the two types of PCAs was used and stacked together to build up a TEM band image. The resulting ten PCA bands image was used in the land cover classification using the maximum likelihood classifier (MLC) method and the resulting overall classification accuracy was 97.5% (Fig. 4). The classification results revealed that olive covered more than third of the studied area (36.4%), followed by the bare soils and citrus, which covered 26.08 and 24.67 % of the studied area, respectively. Lastly, the vegetables covered 12.85 %of the studied area (Table 8). Accordingly, only citrus and olive were selected for evaluation of ET map production using S-SEBI.

Normalized difference vegetation index (NDVI)

The NDVI values of the validation area reported throughout the year are shown in Fig. 5. Citrus and olive reached maximum NDVI values (0.58 and 0.47, respectively) in October, while both reached the minimum NDVI values (0.41 and 0.32, respectively) in June. The spatial distribution of the NDVI at the peak (October), dip (June) and average (February) are shown in Fig. 6.

Calculation of the evaporative fraction Λ

The evaporative fraction was calculated using the surface albedo (Fig. 7) and the land surface temperature LST (Fig. 8). Both the surface albedo and LST for each date have been stacked into one image. Thereafter, the space plot was generated from surface albedo versus LST for the nine Landsat-8 images. Data from the cold edge represented by water locations and from the hot edge from uncultivated dry areas have been collected. These data were used as suggested by Roerink*et al.* (2000) for the calculation of Λ.

Evapotranspiration

Fig. 9 shows the ET value maps in the selected dates in the study area while Fig. 10 shows the averaged ET of citrus and olive throughout the growing season of 2020 calculated from Landsat-8 images. The data revealed that both citrus and olive reached their highest ET in summer and lowest in winter. The average ET for citrus ranged from 2.87 mm/day in February to 7.30 mm/ day in June, while olive ET ranged from 3.22 mm/ day in December to 6.18 in May.

Performance evaluation of S-SEBI

The ET values produced from the CROPWAT-8 model are shown in Fig. 11. The data revealed that both citrus and olive reached their higher ET values in summer and lowest in winter. Nevertheless, the citrus highest ET value was in July (7.45 mm/day) and the lowest in October (2.23 mm/day) and olive reached its highest

Table 7. Acreage of the LC classes

Class	Feddan	%
Citrus	56.36	24.67
Olive	83.14	36.40
Vegetables	29.36	12.85
Bare soil	59.57	26.08
Total	228.43	100.00

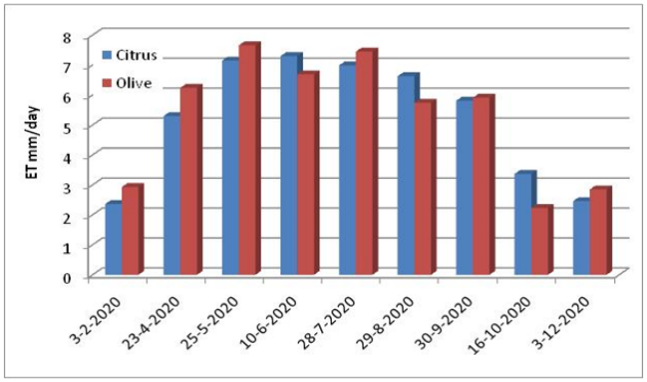

Fig. 10. *Average ET values of citrus and olive in 2020 from the S-SEBI*

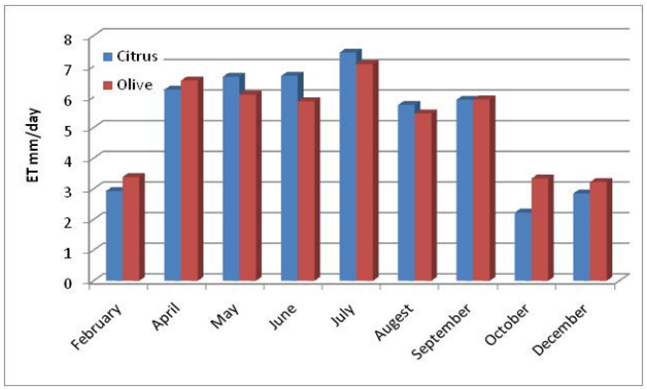

Fig. 11. *Monthly ET values of citrus and olive from CROPWAT model*

value in July (7.07 mm/day) and lowest in December (3.22 mm/day).

The linear regression analysis between the S-SEBI-ET and the CROPWAT-ET for both citrus and olive collectively revealed that the data reached r^2 of 0.82 and RMSE of 0.53 mm/day. On the other hand, processing each crop individually revealed that citrus had r^2 of 0.87 while olive only reached r^2 of 0.77. The same trend was observed when calculating the RMSE. The RMSE was 0.48 mm/day for citrus and 0.58 mm/day for olive. It is worth mentioning that while the area is considered homogenous, the southern part of this area where olive is cultivated, based on field observation, was unproductive in some areas and consequently was leading to the removal of some of the trees and replacing them with field crops. Such a change will affect the ET values calculated from both S-SEBI and CROPWAT.

Conclusion

The present study revealed that the ET estimated using the Landsat-8 and S-SEBI showed a high correlation coefficient (r2 = 0.82) and relatively low RMSE (0.53 mm/day) compared to CROPWAT-ET data. Furthermore, theS-SEBI could easily and effectively document the temporal and spectral ET changes within the study area. It will be easier for decision-makers to utilize the proposed methodology to set up efficient water management for the crop in a selected area with only satellite data and limited meteorological data. The study also recommends *in situ* studies for validation of the proposed methodology.

Conflict of interest

The authors declare that they have no conflict of interest.

REFERENCES

1. Abdel Kader, M.H., Khalifa, H.E., Sheta A.S. & Ibrahim, A.A, (2015). Evapotranspiration estimation using remote sensing data and some climatic models. *J. Soil Sci. and Agric. Eng., Mansoura Univ.,* 6 (11), 1341 – 1354.
2. Allen, R.G., Pereira, L.S., Raes, D. & Smith, M. (1998). Crop evapotranspiration - guidelines for computing crop water requirements. FAO Irrigation and Drainage Paper 56; FAO, Rome, Italy.
3. Allen, R.G., Tasumi, M. & Trezza, R., (2007). Satellite-based energy balance for mapping evapotranspiration with internalized calibration (METRIC) Model. *Journal of Irrigation and Drainage Engineering,* 133(4), 380–394. https://doi.org/10.1061/(ASCE)0733-9437(2007)133:4(380)
4. Ayyad, S., Al Zayed, I. S., Thi Ha V. T. & Ribbe, L. (2019). The Performance of Satellite-Based Actual Evapotranspiration Products and the Assessment of Irrigation Efficiency in Egypt. *Water,* 11(9), 1913-1922.https://doi.org/10.3390/w11091913
5. Basit, A., Khalil, R. Z. & Haque, S. (2018). Application of Simplified Surface Energy Balance Index (S-SEBI) for Crop Evapotranspiration using Landsat 8. *International Archives of the Photogrammetry, Remote Sensing and Spatial Information Sciences*, XLII-1, 33–37.https://doi.org/10.5194/isprs-archives-XLII-1-33-2018.
6. Bastiaanssen, W. G. M.(2000). SEBAL-basedsensible and latent heat fluxes in the irrigated Gediz Basin, Turkey. *Journal of Hydrology,* 229 (1-2), 87-100.https://doi.org/10.1016/S0022-1694(99)00202-4
7. Bezerra, B.G., da Silva, B.B., dos Santos, C.A.C. & Bezerra, J.R.C. (2015). Actual evapotranspiration estimation using remote sensing: comparison of SEBAL and SSEB approaches. *Advances in Remote Sensing*, 4, 234-247.https://doi.org/10.4236/ars.2015.43019.
8. Carlson, T. & Ripley, D. (1997). On the relation between NDVI, fractional vegetation cover, and leaf area index. *Remote Sensing of Environment*,62, 241-252. https://doi.org/10.1016/S0034-4257(97)00104-1.
9. Ezz, H. & Abdelwares M. (2020). Spatial and Temporal Variation of ETo ETO for EGYPT using Remote Sensing. *ARPN Journal of Engineering and Applied Sciences,* 15 (1), 104-112. http://www.arpnjournals.org/jeas/research_papers/rp_2020/jeas_0120_8073.pdf.
10. Foodand Agriculture Organization (2009). CROPWAT 8.0. Edited, Land and Water Development Division, Rome, Italy.
11. Jiang, Z., Huete, A., Chen, J., Chen, Y., Li, J., Yan, G. & Zou, Y. (2006). Analysis of NDVI and scaled difference vegetation index retrievals of vegetation fraction. *Remote Sensing of Environment*. 101. 366-378. https://doi.org/10.1016/j.rse.2006.01.003.
12. Kukla, G. J. (1981). Surface Albedo. In: Berger, A. (eds) Climatic Variations and Variability: Facts and Theories. *NATO Advanced Study Institutes Series*, Vol 72. Springer, Dordrecht. https://doi.org/10.1007/978-94-009-8514-8_4.
13. Kumar, U., Rashmi, Chatterjee, C., Raghuwanshi, N.S., (2021). Comparative evaluation of simplified surface energy balance index-based actual ET against lysimeter data in a Tropical River basin. *Sustainability,* 13, 13786. https://doi.org/10.3390/su132413786.
14. Kumar, U., Sahoo, B., Chatterjee, C. & Raghuwanshi, N. S. (2020). Evaluation of simplified surface energy balance index (S-SEBI) method for estimating actual evapotranspiration in Kangsabati Reservoir Command using Landsat 8 imagery. *Journal of the Indian Society of Remote Sensing,* 48(10), 1421–1432. https://doi.org/10.1007/s12524-020-01166-9.
15. Li, Z. L., Tang, R., Wan, Z., Bi, Y., Zhou, C., Tang, B., Yan, G. & Zhang, X. (2009). A review of current methodologies for regional evapotranspiration estimation from remotely sensed data. *Sensors*, 9(5), 3801-3853. https://doi.org/10.3390/s90503801.
16. Alves, E.R.A., de Freita, I. G. F., Gomes, H. B. , Silva, F. D. & dos Santos, M. N.(2017). Using Landsat-8 images in the estimative of surface radiation balance. *Journal of Hyperspectral Remote Sensing,* 7(2), 91-100.
17. Makar R. S., Shahin Sahar A., El-Nazer Mostafa & Wheida Ali (2022). Development of a PCA-based land use/land cover classification utilizing Sentinel-2-time series. Middle

East Journal of Agriculture Research, 11(2):630-637. https://doi.org/10.36632/mejar/2022.11.2.42.

18. Mondal, I., Thakura, S., Deb, A. & Dea, T. K. (2022). Application of the METRIC model for mapping evapotranspiration over the Sundarban Biosphere Reserve, India. *Ecological Indicators*, 136, 108553. https://doi.org/10.1016/j.ecolind.2022.108553
19. Rawata, K.S., Singh, S.K., Bala, A. & Szabo, S., (2019). Estimation of crop evapotranspiration through spatial distributed crop coefficient in a semi-arid environment. *Agric. Water Manag.,* 213,922-933.https://doi.org/10.1016/j.agwat.2018.12.002.
20. Reyes-González, A., Kjaersgaard, J., Trooien, T., Reta-Sánchez, D. G., Sánchez-Duarte, J. I., Preciado-Range, P. & Fortis-Hernández, M. (2019). Comparison of leaf area index, surface temperature, and actual evapotranspiration estimated using the METRIC model and insitu measurements. *Sensors*, 19(8), 1857-1878. https://doi.org/10.3390/s19081857
21. Rodrigues, G.C. & Braga, R.P., (2021). Estimation of daily reference evapotranspiration from NASA POWER reanalysis products in a hot summer Mediterranean climate. *Agronomy,* 11, 2077-2091. https://doi.org/10.3390/agronomy11102077.
22. Roerink, G.J., Su, Z. & Menenti, M. (2000). S-SEBI: A simple remote sensing algorithm to estimate the surface energy balance. *Physics and Chemistry of the Earth, Part B: Hydrology, Oceans and Atmosphere*, 25(2), 147-157. https://doi.org/10.1016/S1464-1909(99)00128-8
23. Rouse, J.W., R.H. Haas, J.A. Schell & D. W. Deering (1974). Monitoring vegetation systems in the Great Plains withERTS, In: S.C. Freden, E.P. Mercanti, and M. Becker (eds) Third Earth Resources Technology Satellite–1 Syposium. Volume I: Technical Presentations, NASA SP-351, NASA, Washington, D.C., pp. 309-317
24. Senay, G.B., Bohms, S., Singh, R.K., Gowda, P.H., Velpuri, N.M., Alemu, H. & Verdin, J.P. (2013). Operational evapotranspiration mapping using remote sensing and weather datasets: A new parameterization for the SSEB approach. *Journal of the American Water Resources Association (JAWRA),* 49(3), 577–591. https://doi.org/10.1111/jawr.12057
25. Sobrino, J. A. & Raissouni, N., (2000). Toward remote sensing methods for land cover dynamic monitoring: application to Morocco. *Int. J. Remote Sens.,* 21(2), 353-366. https://doi.org/10.1080/014311600210876.
26. Sobrino, J. A., El Kharraz, J. & Li, Z. L. (2003). Surface temperature and water vapour retrieval from MODIS data. *International Journal of Remote Sensing*,24 (24),5161-5182. https://doi.org/10.1080/0143116031000102502
27. Sobrino, J. A., Raissouni, N., Olioso, A., Hasager, C. B., Belaid, M., Abdel Rahman, S. & Chehbouni, A., (2001). WATERMED - Water use efficiency in natural vegetation and agricultural areas by Remote sensing in the Mediterranean basin. In *IGARSS 2001. Scanning the Present and Resolving the Future. Proceedings. IEEE 2001 International Geoscience and Remote Sensing Symposium (Cat. No.01CH37217)*, 2001, pp. 3158-3160 vol.7, Sydney, Australia, 9–13 July, 2001. https://doi.org/10.1109/IGARSS.2001.978289.
28. Sobrino,J. A., Jiménez-Muñoz, J. C.,Sòria, G., and Romaguera, M.,Guanter, L., Moreno J., Plaza, A. & Martínez, P. (2008). Land surface emissivity retrieval from different VNIR and TIR sensors. *IEEE Transactions on Geoscince and Remote Sensing,* 46(2), 316-327. https://doi.org/10.1109/TGRS.2007.904834.
29. Sobrino, J.A.; Souza daRocha, N., Skokovi´c, D.,SuélenKäfer, P., López-Urrea, R., Jiménez-Muñoz, J.C. & Alves Rolim, S.B. (2021). Evapotranspiration Estimation withthe S-SEBI Method from Landsat 8Data against LysimeterMeasurements at the Barrax Site,Spain. *Remote Sens.,* 13: 3686-3703.https://doi.org/10.3390/rs13183686.
30. United States Geological Survey (2019). Landsat 8 (L8), Data Users Handbook. EROS Sioux Falls, South Dakota. LSDS-1574, Version 5.0. https://d9-wret.s3.us-west-2.amazonaws.com/assets/palladium/production/s3fs-public/atoms/files/LSDS-1574_L8_Data_Users_Handbook-v5.0.pdf.
31. Vozhehova R. A., Lavrynenko Y. O., Kokovikhin S. V., Lykhovyd P. V., Biliaieva I. M., Drobitko A. V. & Nesterchuk V. V. (2018). Assessment of the CROPWAT 8.0 software reliability for evapotranspiration and crop water requirements calcu-lations. *Journal of Water and Land Development.* 39, 147–152. https://doi.org/10.2478/jwld-2018-0070.